

A CATALOGUE OF FIELD HORIZONTAL BRANCH STARS ALIGNED WITH HIGH VELOCITY CLOUDS

CHRISTOPHER THOM¹ AND BRAD K. GIBSON¹

Centre for Astrophysics and Supercomputing, Swinburne University of Technology, PO Box 218, Hawthorn, Victoria, 3122, Australia

NORBERT CHRISTLIEB²

Hamburger Sternwarte, Universität Hamburg, Gojenbergsweg 112, D-21029 Hamburg, Germany

Draft version November 6, 2018

ABSTRACT

We present a catalogue of 430 Field Horizontal Branch (FHB) stars, selected from the Hamburg/ESO Survey (HES), which fortuitously align with high column density neutral hydrogen (H I) High-Velocity Cloud (HVC) gas. These stars are ideal candidates for absorption-line studies of HVCs, attempts at which have been made for almost 40 years with little success. A parent sample of 8321 HES FHB stars was used to extract H I spectra along each line-of-sight, using the H I Parkes All-Sky Survey. All lines-of-sight aligned with high velocity H I emission with peak brightness temperatures greater than 120 mK were examined. The H I spectra of these 430 probes were visually screened and cross-referenced with several HVC catalogues. In a forthcoming paper, we report on the results of high-resolution spectroscopic observations of a sample of stars drawn from this catalogue.

Subject headings: Stars: horizontal-branch — ISM: clouds — Galaxy: halo — Galaxy: evolution

1. INTRODUCTION

Discovered by Muller et al. (1963) over 40 years ago, High-Velocity Clouds (HVCs) are H I clouds with velocities that do not conform to simple models of Galactic rotation (e.g. Wakker & van Woerden 1997, and references therein). Since their discovery, HVC distances (and origins) have been the source of much debate, with various scenarios suggested. Shapiro & Field (1976) proposed the existence of a “Galactic Fountain” to explain the observed soft X-ray background and O VI absorption lines. This process, in which hot gas is driven up into the halo by supernovae and stellar winds, which then condenses and falls back onto the disk, was linked by Bregman (1980) to the HVCs (see also de Avillez 2000). Others have suggested they may be the result of tidal disruption of satellite galaxies, e.g. the Magellanic Stream (Putman et al. 2003). Perhaps they are the infalling source of star formation fuel long required by chemical evolution models (e.g. Fenner & Gibson 2003)? Oort (1966) first suggested that some subset of HVCs may be at much larger distances, being the remnants of the galaxy formation process (a suggestion revived by Blitz et al. 1999). Other authors have proposed that the smaller, isolated Compact HVCs (CHVCs) may be explained under this scenario (e.g. de Heij et al. 2002a), suggesting that such objects may also be observable around M31 with sensitive H I observations. Subsequent observations toward M31 have successfully detected HVC-analogs (Thilker et al. 2004), whilst others have failed to find them in searches of Local Group analogues (Pisano et al. 2004).

It is clear that to establish a definitive theory describing HVCs the largely unknown distances are a key element. Many physical properties scale with the distance; physical size ($\propto d$), mass ($\propto d^2$), density ($\propto d^{-1}$) and pressure ($\propto d^{-1}$) for example. Since HVCs do

not conform to models of Galactic rotation, we cannot use those models to derive distances from their observed velocities. Hence another method is required. A distance limit may be set by high-resolution absorption spectroscopy (Danly et al. 1993; Schwarz et al. 1995; van Woerden et al. 1999). If a star is located behind the HVC, the stellar spectrum should contain the imprint of the HVC at the (known) velocity of the cloud. A sufficiently high resolution spectrum should be able to resolve such features. Detection of these absorption lines indicates the star is behind the cloud, and an upper distance limit is set, namely the distance to the star.

The interpretation of non-detections is more challenging and is succinctly summarised by Wakker & van Woerden (1997) (see their Fig. 4). Several possibilities must be taken into account before one can be convinced that the lack of an optical HVC absorption feature indicates that the star is in front of the HVC, and sets a significant lower distance limit. HVCs have been shown to have large column density variations over small (arcmin) angular scales (e.g. Wakker & Schwarz 1991). Since HVCs are usually identified in H I surveys with large beam sizes, high-resolution (interferometric) radio imaging is necessary, to ensure the line-of-sight does not pass through a “sucker hole” in the cloud, missing the expected high column density gas. If the alignment is favorable, we also require sufficiently high metallicity intervening gas (a typical value for HVCs is $\sim 0.1 - 0.3$ solar; see Wakker (2001)); clearly if this is not the case, there will be no metal ions to create an absorption line. Further, knowledge of the gas metallicity comes from other lines-of-sight, so we must assume that there are no abundance variations within the cloud.

Optical absorption line studies are often conducted using the Ca II H and K lines ($\lambda\lambda 3968.469 \text{ \AA}$ and 3933.663 \AA respectively). These two resonance lines have high oscillator strengths and thus should be easily de-

tectable. Prata & Wallerstein (1967) were the first to specifically target the HVCs (unsuccessfully) using absorption line studies, with Kepner (1968) producing the first catalogue of early-type stars aligned with HVCs. Despite almost 40 years of efforts by various groups, only a handful of stellar absorption line studies have successfully detected HVC absorption features¹, providing firm upper limits. van Woerden et al. (1999) detected HVC “Chain A” in Ca II absorption in the optical spectrum of the RR Lyrae star AD UMa, giving a maximum distance of 10 kpc. A few years earlier, Danly et al. (1993) used the *IUE* satellite to detect the HVC Complex M in the UV resonance lines O I, C II and Si II toward the early-type star BD + 38°2182, limiting the HVC to $z < 4.4$ kpc.

Field Horizontal Branch (FHB) stars are valuable probes for distance determination work, for two primary reasons: (i) Their intrinsic luminosity means that sufficiently high signal-to-noise optical spectra can be obtained for distant halo FHB stars ($d \geq 20$ kpc), meaning they can act as useful and interesting discriminators of the various origin scenarios, and (ii) Being hot stars, their spectra are relatively free of intrinsic absorption features, making the detection and interpretation of the HVC absorption features relatively straightforward. Previous authors have also successfully employed RR Lyrae stars (van Woerden et al. 1999) or bright B-stars in the ultraviolet (Danly et al. 1993) and optical (Smoker et al. 2004).

Here we present a table of 430 FHB stars which align with H I gas at high velocities, and the associated H I spectra and moment maps. These stars are ideal for high-resolution optical spectroscopy and distance determinations. Section 2 gives the details about the selection of HVC distance probes from the HES FHB catalogue of Christlieb et al. (2005, hereafter C05). The catalogue of HVC distance probes is presented in Section 3. A brief conclusion is given in Section 4. The full catalogue plus H I spectra and summed intensity moment maps towards each star in the catalogue are presented in the online edition.

2. STELLAR SELECTION AND MATCHING

We have taken as our input sample, the C05 catalogue of 8321 FHB stars selected from the Hamburg/ESO Survey, which has been shown to have contamination from high-gravity main-sequence stars of $< 16\%$. For each stellar line-of-sight, an H I spectrum was extracted from the H I Parkes² All-Sky Survey (HIPASS; Barnes et al. 2001; Putman et al. 2002, hereafter P02) and any emission above a threshold of 0.15 Jy/Beam at high velocities ($|v_{LSR}| \geq 90$ km s⁻¹) identified. This threshold corresponds to a brightness temperature threshold of 0.12 K for the Parkes Multibeam used for the HIPASS survey (e.g. Putman et al. 2003) and is set by the level at which Ca II absorption lines are expected to be detectable in optical spectra (see Sec 2.6). All lines-of-

¹ There is also a large body of ultraviolet absorption line detections against stellar and extra-galactic sources. These ionized high-velocity clouds in some cases align with H I HVCs, in some cases not. See e.g. Sembach et al. (2003) for details.

² The Parkes telescope is part of the Australia Telescope which is funded by the Commonwealth of Australia for operation as a National Facility managed by CSIRO.

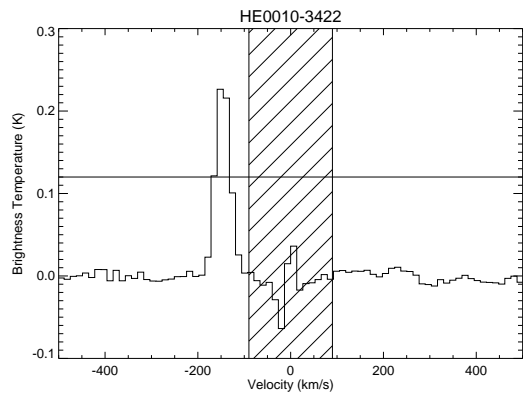


FIG. 1.— Example H I spectrum of a stellar line-of-sight meeting the selection criteria. The horizontal line shows the brightness temperature cut-off, while the shaded region indicates velocity selection criteria. Note that the HIPASS data is unreliable in the vicinity of the Galactic emission near 0 km s⁻¹. The HIPASS spectra are extracted spatially averaging a 3x3 box around the closest pixel to the specified coordinate.

sight meeting these criteria were then screened by eye to reject obvious problems. In all cases, these were due to the wings of emission features well below the $|v_{LSR}| \geq 90$ km s⁻¹ limit extending outside this range above the level of 0.12 K. H I moment maps were created from the HIPASS data cubes around each line of sight, and the positions were matched against several HVC catalogues.

2.1. The Hamburg/ESO Survey

We briefly review the salient points of the HES, while a fuller description of the survey and its stellar products may be found elsewhere (e.g. Wisotzki et al. 1996, C05). Originally a survey for bright quasars, the HES is an objective prism survey which covers a large fraction of the southern extra-galactic sky ($\delta < +2.5^\circ$; $|b| \gtrsim 30^\circ$) to a limiting magnitude of $B \lesssim 18.0$. As well as finding quasars, it has also become a valuable resource for identifying many different classes of interesting stars; e.g. Carbon stars (Christlieb et al. 2001a), White Dwarfs (Christlieb et al. 2001b), metal-poor halo stars (e.g. Christlieb 2003) and FHB stars (C05). Selection of the FHB stars was made first on the basis of a color cut. The second step involved automated selection criteria based on the summed Balmer line equivalent widths and the Strömgren c_1 index. This process resulted in 8321 stars, which have been shown to have a contamination from, e.g. higher surface gravity A-stars, of $< 16\%$. See C05 for further details.

2.2. Spectrum Extraction

To identify stars aligned with HVCs, HIPASS H I spectra for all stellar lines-of-sight were first extracted from the HIPASS HVC cubes. These cubes were produced from the HIPASS data by P02 using the *MINMED5* bandpass calibration, which recovers much of the extended emission lost in the original HIPASS bandpass calibration; since the survey was originally designed for point sources, this loss was not a critical issue. Nevertheless, when emission extends spatially to fill more than $\sim 6^\circ$ of a full HIPASS 8° declination scan, the calibration

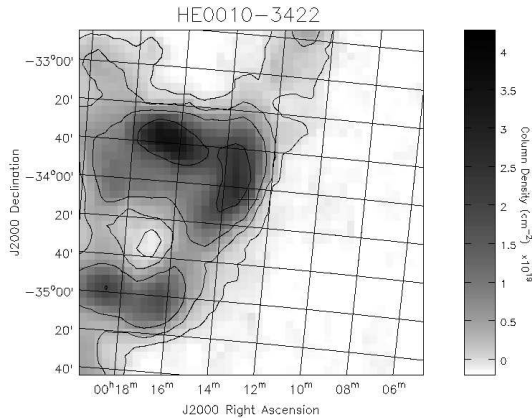


FIG. 2.— Example moment map of the area around HE 0010–3422, the line-of-sight shown in Fig 1. Neutral hydrogen contours are drawn at 2.0×10^{18} , 5.0×10^{18} , 1.0×10^{19} , 2.5×10^{19} , 5.0×10^{19} and $1.0 \times 10^{20} \text{cm}^{-2}$

will not be accurate e.g. for data close to the Galactic plane (see Putman et al. 2003, for details).

The *miriad* task *mbspect* was used to extract the spectra, averaging spatially over a 3×3 pixel box (approximately the HIPASS beam size of 15.5 arcmin; HIPASS pixels are 4 arcmin). *mbspect* uses the nearest pixel to the specified coordinate. All spectra containing emission above the level of 0.12 K at velocities $|v_{LSR}| \geq 90 \text{ km s}^{-1}$ were automatically flagged. An example of such a spectrum is shown³ in Fig 1. We plot only the velocity range $-500 - +500 \text{ km s}^{-1}$ since this is the range occupied by nearly all Galactic HVCs⁴. The associated moment map is shown in Fig 2 (see Section 2.3 for details).

To create the final FHB/HVC catalogue, the spectra for these 430 lines-of-sight were then visually inspected to reject obvious noise artefacts. In some cases, the peak flux was at an absolute velocity less than the enforced 90 km s^{-1} limit, while significant emission was still present outside this range. In these cases, stars were retained if the channel(s) outside the 90 km s^{-1} boundary had a flux comparable to the peak value. Fig 3 shows an example of such a case. In these cases, the peak emission with $|v_{LSR}| \geq 90 \text{ km s}^{-1}$ was recorded.

During screening, it was noted that some spectra contained multiple high-velocity emission components. In cases where these were not immediately identifiable as the same cloud, a separate entry in Table 3 was recorded. These multiple components were flagged in the catalogue and separate moment maps produced. Obviously, separate H I spectra are not required, although the spectra are repeated for completeness. In all but a few cases, these doubles are flagged as associated with the Magellanic Stream (see Section 2.4). HE 1008–0438 also aligns by chance with the galaxy HIPASS J1010-04. The star HE 0053–3740 was found to align with a Sculptor Group galaxy and was excluded. HE 0056–4043 shows a noise spike at $\sim -410 \text{ km s}^{-1}$ which is evident in the HIPASS data cubes.

³ Similar figures are provided for all probes in Table 3 in Figs. 5 – 148 of the online version.

⁴ Note that Thilker et al. (2004) have found HVCs associated with M31 at velocities more negative than the -500 km s^{-1} limit.

TABLE 1
MAGELLANIC STREAM REGIONS.

Region	l (deg)	b (deg)	v_{LSR} (km s^{-1})
1	–	$b \leq -70$	$-300 \leq v \leq 300$
2	$270 \leq l \leq 315$	$-70 \leq b \leq -20$	$70 \leq v \leq 400$
3	$315 \leq l \leq 345$	$-70 \leq b \leq -50$	$70 \leq v \leq 200$
4	$45 \leq l \leq 110$	$-70 \leq b \leq -60$	$-320 \leq v \leq -130$
5	$65 \leq l \leq 110$	$-60 \leq b \leq -48$	$-390 \leq v \leq -200$
6	$65 \leq l \leq 110$	$-48 \leq b \leq -33$	$-390 \leq v \leq -250$

NOTE. — Lines-of-sight in these regions, with velocities consistent with the limits specified, are flagged as associated with the Magellanic Stream.

2.3. Moment Maps

In order to visualize the spatial locations of the stars with respect to the gas, summed-intensity moment maps of a region approximately $3^\circ \times 3^\circ$ centered around each probe were created. Moment maps were generated by summing the velocity channel containing the peak flux outside the $|v_{LSR}| \geq 90 \text{ km s}^{-1}$ boundary and the two adjacent channels. This summed width equates to 39.6 km s^{-1} , which is approximately the 36 km s^{-1} median FWHM of the HIPASS HVCs (P02) (note, though, that this median is almost certainly an overestimate of the true value and a product of the coarse velocity resolution of the HIPASS data). Maps were converted to column densities using the relation $N(HI) = 1.823 \times 10^{18} \int T_b dv$ (Dickey & Lockman 1990). Onto these moment maps, contours were drawn at H I column densities of 2.0×10^{18} , 5.0×10^{18} , 1.0×10^{19} , 2.5×10^{19} , 5.0×10^{19} and 1.0×10^{20} . The positions of the FHB stars are marked by a “+” in the centers of these images, one example of which is shown⁵ in Figure 2.

2.4. Cloud Matching and the Magellanic Stream

One of the most prominent features in the southern radio sky at 21 cm is the Magellanic Stream (MS). We wanted to differentiate the entries that probe gas possibly associated with the Stream, from those probing other HVCs. In this vein we follow the spatial and kinematic regions defined in Figs. 5 and 7 respectively of Putman et al. (2003). Table 1 shows the regions we adopt as being associated with the Stream. Probes within these regions are flagged in the catalogue. Note that exact definitions of which clouds are associated with the Stream are difficult and somewhat subjective – the definitions here should be considered as a guide only. Further, there is some overlap between the Stream as defined here and the Sculptor group of galaxies. Despite this attempted flagging, some of the CHVCs and semi-compact HVCs catalogued by P02 and de Heij et al. (2002b, hereafter D02) are also flagged as Stream-related. Since their origin has been proposed to be quite different from that of the large complexes, and given the imperfect nature of the MS flagging, these probes may prove quite interesting and are not excluded from Table 3.

⁵ Similar figures are provided for all probes in Table 3 in Figs. 5 – 148 of the online version.

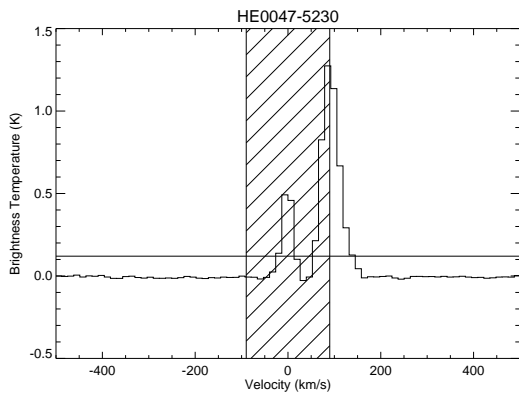


FIG. 3.— Example H I spectrum of a stellar line-of-sight with peak flux inside the $|v_{LSR}| \geq 90 \text{ km s}^{-1}$ boundary. Note the clean separation from the Galactic emission at low velocity.

Using the HVC catalogues published by P02, D02 and Wakker & van Woerden (1991, hereafter WvW91) we have attempted to identify which clouds are associated with each detection. From P02, we use both the tables of HVCs, plus their table of XHVCs – clouds which have emission at high velocities, but which clearly link to emission at lower deviation velocities⁶. Since clouds have arbitrary shapes, this is a difficult process.

In general, the optimal solution to the problem of associating stellar lines-of-sight with individual clouds would be to obtain component lists for all clouds in the desired catalogue (i.e. which pixels make up a particular cloud). Unfortunately, such lists are not available for the catalogues we searched, so another strategy was required.

From the tables of HVCs and XHVCs reported in P02, we took a position and angular size. Assuming a circular cloud, we found all clouds which encompass the stellar position. We then required that the velocity measured in the HIPASS spectrum and the velocity of the cloud differ by no more than the FWHM of the cloud. For the few cases where multiple clouds met these criteria, the data cubes were examined and it was immediately apparent which was the correct entry.

The D02 catalogue is very similar in structure; indeed, the same algorithm was used by P02 to create the HIPASS catalogue. The one exception is that D02 do not publish the size of individual clouds, based on the number of associated pixels, as do P02. They do, however, provide the major and minor axes of an ellipse which is fit to half the peak flux level. We used the major axis length to search a circular area around the reported cloud position. To avoid associating some clouds with large fractions of the sky (i.e. some clouds have major axes up to $\sim 165^\circ$), we limited the search radius to 10 deg. The same FWHM velocity criteria as above were also applied.

For the clouds in the catalogue of WvW91 the same process was repeated. Since those authors do not tabulate the FWHM for individual clouds, we assumed a FWHM of 36 km s^{-1} , based on the global properties of the HIPASS HVCs listed in Table 2 of P02.

⁶ Deviation velocity is the degree to which a velocity deviates from the maximum allowed by Galactic rotation in that direction (Wakker 1991).

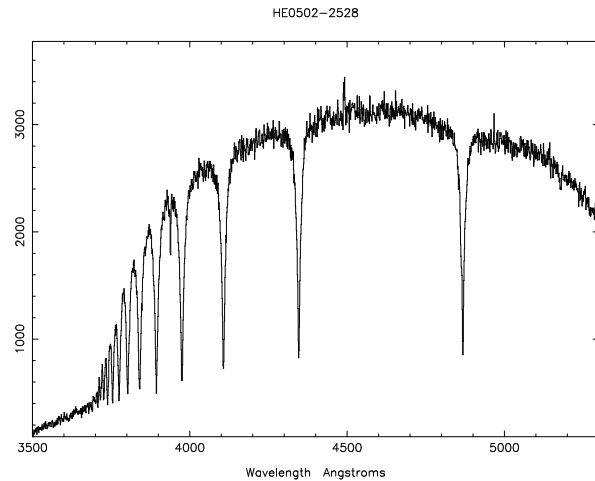


FIG. 4.— Medium resolution spectrum of the FHB star HE 0502–2528. Note the general lack of metal absorption lines, which could confuse the interpretation of any potential HVC.

2.5. Stellar Velocities

It will be difficult or impossible to detect HVC absorption features in high resolution optical spectra if the velocity of the gas and stellar radial velocity (RV) are too close. In this case, stellar absorption will dominate the spectrum and the HVC feature will be lost. As part of a separate program, we have obtained medium-resolution spectra of 18 stars in our catalogue using the Double-Beam Spectrograph on the SSO 2.3m. An example of such a spectrum is shown in Fig. 4. Note the general lack of metal absorption lines, with the exception of the stellar Ca II K line at 3933.663 \AA . From these spectra we obtained radial velocities by fitting Sersic profiles to the $H\beta$, $H\gamma$ and $H\delta$ Balmer lines. Table 2 lists the average stellar RV corrected to the Local Standard of Rest (LSR) frame, along with the H I velocity and the absolute difference of the two. Clearly, the greater the difference between the stellar and HVC features, the easier a detection will be and we suggest that a velocity difference of greater than $\sim 50 \text{ km s}^{-1}$ will be needed. Such observations must be of sufficient resolution (i.e. $R = 40000 - 60000$, corresponding to $\sim 7.5 - 5 \text{ km s}^{-1}$ at Ca II K) to resolve the separation between the HVC, stellar and disk absorption features.

We have performed a simple simulation to estimate, to first-order, the percentage of halo stars that are expected to have velocities within 50 km s^{-1} of an HVC. Stars in the halo are drawn from a population with a total dispersion of $\sigma \simeq 200 \text{ km s}^{-1}$. Assuming an isotropic distribution of velocities, a single projection (e.g. the line-of-sight component) will then follow a Gaussian distribution with $\sigma_{LOS} \simeq 200/\sqrt{3} \simeq 120 \text{ km s}^{-1}$. We randomly generated stellar velocities according to such a distribution. For each of these velocities, we also generated a random HVC velocity using the HIPASS HVC velocity distribution (e.g. Fig 10 of Putman et al. 2002). Comparing these two velocities, we find that they are within 50 km s^{-1} of each other $\sim 13\%$ of the time. It should be noted, however, that this is a global average; clearly HVCs with lower velocities will have, on average, a chance velocity alignment more often, while very high

TABLE 2
STELLAR VELOCITY COMPARISONS

HE name	Radial Velocity (km s^{-1})	v_{LSR} (km s^{-1})	v_{diff} (km s^{-1})
HE 0003–5248	+058	+112	–054
HE 0046–3255	–012	+112	–124
HE 0056–3330	+113	–191	+304
HE 0157–5126	+047	+165	–118
HE 0420–5405	+070	+099	–029
HE 0502–2528	+370	+099	+271
HE 0504–2509	+066	+112	–046
HE 0506–2530	+204	+125	+079
HE 0932–0404	+257	+152	+105
HE 1004–0516	+219	+112	+107
HE 1027–2625	+261	+218	+043
HE 1045–2550	+125	+178	–053
HE 1318–2555	–035	+112	–147
HE 1323–2511	+182	+112	+070
HE 2155–2243	–098	–139	+041
HE 2200–2222	+141	–099	+240
HE 2242–6106	+094	+112	–018
HE 2304–3858	–038	–112	+074

NOTE. — Stellar velocity comparisons for stars with medium resolution optical observations. Listed are the LSR stellar and H I velocities. A minimum separation of 50 km s^{-1} is suggested for a star to be useful for high resolution optical observations. Stellar radial velocities have been corrected to the LSR frame using the IRAF task *rvcorrect*, which assumes a solar motion of 20 km s^{-1} towards $\alpha = 18:00:00$, $\delta = 30:00:00$ (B1900)

velocity HVCs will suffer such problems less than the average.

2.6. Optical Detections

In order to detect an absorption line in the optical, there must be a sufficient number of absorbing atoms along the line-of-sight. Assuming an optically thin gas, Savage & Sembach (1996) give a relation between the column density N and the equivalent width of the absorption line W_λ . Since an H I column density can be measured from the HIPASS spectra by integrating over the HVC emission line, if the ratio of Ca^+ ions to H I atoms, $N(\text{Ca}^+)/N(\text{H I})$ is known, we can predict the equivalent width of the Ca II absorption features. It should be noted that an accurate determination of $N(\text{Ca}^+)/N(\text{H I})$ is important, since this quantity can vary by up to 2 orders of magnitude from cloud to cloud (Wakker 2001)⁷. For the lowest column density features in Table 3, the expected equivalent width is $\sim 20 \text{ m}\text{\AA}$, which should be detectable using large telescopes in a reasonable amount of time.

3. THE CATALOGUE

After these selection criteria were applied, we had a total of 430 stars probing sufficiently dense HVC gas.

⁷ However Wakker & Mathis (2000) show a relation between the Ca II abundance and column density with much less variation at

These stars are listed in Table 3. The table contains the following columns: Column (1) gives the running number. Column (2) indicates the HES name of the star. Multiple components in a single line-of-sight have separate entries and are numbered. Columns (3) and (4) list the right ascension and declination (J2000) of the stellar probe, with Columns (5) and (6) showing the corresponding Galactic coordinates of the star. The large gap between RA $\sim 13:30 - 21:30$ is due to the HES avoidance of the Galactic plane. Column (7) gives the HES B magnitude, which is accurate to $\sim 0.2 \text{ mag}$ (Wisotzki et al. 2000). The distance to the star (in kpc) is shown in column (8) and is taken directly from C05. Briefly, the distance was derived by those authors by estimating the absolute magnitude M_V from the $B-V$ color. A metallicity correction was applied based on an assumed average halo metallicity and the distance moduli computed. For any higher gravity A-star contaminants, this distance will be incorrect. The peak brightness temperature (in K) is shown in column (9); P02 quote a 5σ sensitivity of 0.04 K . Column (10) shows the H I column density along the line-of-sight, which was measured from the moment maps. The LSR velocity (km s^{-1}) of the peak H I emission outside the $|v_{LSR}| \geq 90 \text{ km s}^{-1}$ zone is given in column (11). This is the velocity of the HIPASS channel containing the peak flux – no attempt at profile fitting was made. The HIPASS velocity resolution is 26.4 km s^{-1} after hanning smoothing. An asterisk in column (12) indicates an association with the Magellanic Stream, (see Sec. 2.4). The matches to the P02 HVCs and XHVCs, the WvW91 HVCs and the D02 HVCs are given in columns (13), (14), (15) and (16) respectively. For the P02 and D02 catalogues, the original nomenclature classifying the cloud (e.g. HVC, CHVC, HVC: etc) has been retained.

4. CONCLUSION

We have presented a catalogue of FHB stars, selected from the Hamburg/ESO Survey, that fortuitously align with high-velocity H I gas. These stars should make ideal candidates for echelle spectroscopy. Such observations offer the possibility of detecting the doppler-shifted absorption features in the spectrum, placing an upper limit on the distance to the HVC. In a similar fashion, non-detections place lower limits on the distance. Distance limits will help to resolve the question of the origins of HVCs and their role in the formation and evolution of Galaxies.

The financial support of the Australian Research Council, through its Discovery Project and Linkage International Award schemes, is gratefully acknowledged. We thank the scientific editor, W. Butler Burton, for his extensive and helpful suggestions.

a given column density.

REFERENCES

- Barnes, D. G., Staveley-Smith, L., de Blok, W. J. G., Oosterloo, T., Stewart, I. M., Wright, A. E., Banks, G. D., Bhathal, R., Boyce, P. J., Calabretta, M. R., Disney, M. J., Drinkwater, M. J., Ekers, R. D., Freeman, K. C., Gibson, B. K., Green, A. J., Haynes, R. F., te Lintell Hekkert, P., Henning, P. A., Jerjen, H., Juraszek, S., Kesteven, M. J., Kilborn, V. A., Knezek, P. M., Koribalski, B., Kraan-Korteweg, R. C., Malin, D. F., Marquarding, M., Minchin, R. F., Mould, J. R., Price, R. M., Putman, M. E., Ryder, S. D., Sadler, E. M., Schröder, A., Stootman, F., Webster, R. L., Wilson, W. E., & Ye, T. 2001, MNRAS, 322, 486
- Blitz, L., Spergel, D. N., Teuben, P. J., Hartmann, D., & Burton, W. B. 1999, ApJ, 514, 818
- Bregman, J. N. 1980, ApJ, 236, 577
- Christlieb, N. 2003, Rev. Mod. Astron., 16, 191, astro-ph/0308016

- Christlieb, N., Beers, T. C., Thom, C., Wilhelm, R., Rossi, S., Flynn, C., Wisotzki, L., & Reimers, D. 2005, *A&A*, 431, 143
- Christlieb, N., Green, P., Wisotzki, L., & Reimers, D. 2001a, *A&A*, 375, 366
- Christlieb, N., Wisotzki, L., Reimers, D., Homeier, D., Koester, D., & Heber, U. 2001b, *A&A*, 366, 898
- Danly, L., Albert, C. E., & Kuntz, K. D. 1993, *ApJ*, 416, L29+
- de Avillez, M. A. 2000, *Ap&SS*, 272, 23
- de Heij, V., Braun, R., & Burton, W. B. 2002a, *A&A*, 392, 417
- . 2002b, *A&A*, 391, 159
- Dickey, J. M. & Lockman, F. J. 1990, *ARA&A*, 28, 215
- Fenner, Y. & Gibson, B. K. 2003, *Publ. Astr. Soc. Aus.*, 20, 189
- Kepner, M. E. 1968, *Bull. Astron. Inst. Netherlands*, 20, 98
- Muller, C. A., Oort, J. H., & Raimond, E. 1963, *Comptes Rendus de l'Académie des Sciences Paris*, 257, 1661
- Oort, J. H. 1966, *Bull. Astron. Inst. Netherlands*, 18, 421
- Pisano, D. J., Barnes, D. G., Gibson, B. K., Staveley-Smith, L., Freeman, K. C., & Kilborn, V. A. 2004, *ApJ*, 610, L17
- Prata, S. & Wallerstein, G. 1967, *PASP*, 79, 202
- Putman, M. E., de Heij, V., Staveley-Smith, L., Braun, R., Freeman, K. C., Gibson, B. K., Burton, W. B., Barnes, D. G., Banks, G. D., Bhathal, R., de Blok, W. J. G., Boyce, P. J., Disney, M. J., Drinkwater, M. J., Ekers, R. D., Henning, P. A., Jerjen, H., Kilborn, V. A., Knezek, P. M., Koribalski, B., Malin, D. F., Marquarding, M., Minchin, R. F., Mould, J. R., Oosterloo, T., Price, R. M., Ryder, S. D., Sadler, E. M., Stewart, I., Stootman, F., Webster, R. L., & Wright, A. E. 2002, *AJ*, 123, 873
- Putman, M. E., Staveley-Smith, L., Freeman, K. C., Gibson, B. K., & Barnes, D. G. 2003, *ApJ*, 586, 170
- Savage, B. D. & Sembach, K. R. 1996, *ARA&A*, 34, 279
- Schwarz, U. J., Wakker, B. P., & van Woerden, H. 1995, *A&A*, 302, 364
- Sembach, K. R., Wakker, B. P., Savage, B. D., Richter, P., Meade, M., Shull, J. M., Jenkins, E. B., Sonneborn, G., & Moos, H. W. 2003, *ApJS*, 146, 165
- Shapiro, P. R. & Field, G. B. 1976, *ApJ*, 205, 762
- Smoker, J. V., Lynn, B. B., Rolleston, W. R. J., Kay, H. R. M., Bajaja, E., Poppel, W. G. L., Keenan, F. P., Kalberla, P. M. W., Mooney, C. J., Dufton, P. L., & Ryans, R. S. I. 2004, *MNRAS*, 352, 1279
- Thilker, D. A., Braun, R., Walterbos, R. A. M., Corbelli, E., Lockman, F. J., Murphy, E., & Maddalena, R. 2004, *ApJ*, 601, L39
- van Woerden, H., Schwarz, U. J., Peletier, R. F., Wakker, B. P., & Kalberla, P. M. W. 1999, *Nature*, 400, 138
- Wakker, B. P. 1991, *A&A*, 250, 499
- . 2001, *ApJS*, 136, 463
- Wakker, B. P. & Mathis, J. S. 2000, *ApJ*, 544, L107
- Wakker, B. P. & Schwarz, U. J. 1991, *A&A*, 250, 484
- Wakker, B. P. & van Woerden, H. 1991, *A&A*, 250, 509
- . 1997, *ARA&A*, 35, 217
- Wisotzki, L., Christlieb, N., Bade, N., Beckmann, V., Köhler, T., Vanelle, C., & Reimers, D. 2000, *A&A*, 358, 77
- Wisotzki, L., Köhler, T., Grootte, D., & Reimers, D. 1996, *A&AS*, 115, 227

TABLE 3
CATALOGUE OF FHB STARS ALIGNED WITH HVCs.

Num	HEname	RA (J2000)	DEC (J2000)	l (deg)	b (deg)	B mag (mag)	Distance (kpc)	T_b (K)	N(H I) (cm^{-2})	v_{LSR} km s^{-1}	MS Flag	HVC
327	HE2129-0202	21:32:31.5	-01:49:20	52.18	-36.127	16.8	14.3	0.13	7.4e+18	+112	-	CHVC#425
328	HE2141-2039	21:44:28.7	-20:25:29	31.44	-46.950	16.3	6.8	0.14	8.3e+18	-178	-	HVC#291
329	HE2153-2323	21:56:32.7	-23:09:24	28.70	-50.416	14.5	4.8	0.25	1.6e+19	-112	-	HVC#283
330	HE2155-2133	21:58:25.9	-21:18:47	31.67	-50.320	16.7	11.9	0.20	1.2e+19	-125	-	HVC#283
331	HE2155-2243	21:58:39.9	-22:29:29	29.92	-50.711	15.3	6.2	0.77	4.8e+19	-139	-	HVC#283
332	HE2200-2222	22:02:54.8	-22:08:06	30.90	-51.551	16.4	10.4	0.39	2.3e+19	-099	-	HVC#283
333	HE2200-2157	22:03:17.4	-21:42:31	31.59	-51.528	17.7	21.5	0.25	1.5e+19	-099	-	HVC#283
334	HE2200-2249	22:03:32.4	-22:35:13	30.26	-51.824	15.7	7.2	0.13	7.7e+18	-099	-	HVC#283
335	HE2235-4908	22:38:52.5	-48:52:38	343.54	-56.474	16.2	9.3	0.22	1.4e+19	+099	*	HVC#1877
336	HE2236-6040	22:39:26.1	-60:25:07	327.61	-49.916	16.7	14.8	0.17	1.1e+19	+099	-	HVC#1727
337	HE2242-6106	22:45:48.5	-60:51:02	326.29	-50.207	14.0	3.9	0.22	1.1e+19	+112	*	HVC#1727
338	HE2247-5811	22:50:18.7	-57:55:22	329.10	-52.619	16.3	12.5	0.15	8.4e+18	+099	*	-
339	HE2248-5733	22:51:17.5	-57:17:54	329.72	-53.132	14.5	5.4	0.21	1.2e+19	+099	*	-
340	HE2249-5740	22:52:46.8	-57:24:30	329.36	-53.204	15.1	6.4	0.49	2.8e+19	+099	*	-
341	HE2251-5755	22:54:18.6	-57:39:02	328.83	-53.197	17.1	16.7	0.50	2.7e+19	+099	*	-
342	HE2252-5943	22:55:25.1	-59:27:39	326.53	-52.025	16.4	12.6	0.20	1.1e+19	+112	*	-
343	HE2253-6056	22:56:35.4	-60:40:07	325.02	-51.258	16.5	12.6	0.20	1.3e+19	+125	*	HVC#1727
344	HE2254-5929	22:57:17.7	-59:13:38	326.52	-52.366	16.2	10.7	0.36	2.1e+19	+112	*	-
345	HE2255-5806	22:58:39.1	-57:50:29	327.92	-53.470	16.7	13.0	0.17	9.7e+18	+152	*	-
346	HE2256-5859	22:59:12.0	-58:43:37	326.80	-52.890	16.8	13.4	0.30	1.7e+19	+138	*	-
347	HE2301-6154	23:04:49.1	-61:38:18	322.80	-51.186	15.9	9.4	0.34	1.8e+19	+099	*	-
348	HE2302-6140	23:05:35.6	-61:24:04	322.93	-51.422	15.5	7.6	0.60	3.4e+19	+099	*	-
349	HE2304-3858	23:07:26.3	-38:41:52	358.27	-65.426	16.4	9.8	0.42	2.5e+19	-112	-	CHVC#1976
350	HE2305-6146	23:08:24.6	-61:30:00	322.41	-51.551	16.9	16.3	0.56	3.3e+19	+099	*	-
351	HE2307+0131	23:09:46.4	+01:47:55	78.63	-52.111	17.4	18.1	0.19	1.1e+19	-310	-	HVC#476
352	HE2307+0125	23:09:58.4	+01:41:38	78.59	-52.227	16.9	14.1	0.15	9.1e+18	-310	-	HVC#476
353	HE2308-3256	23:11:37.6	-32:39:58	12.50	-67.736	17.5	20.3	0.16	8.9e+18	-165	-	CHVC#129

NOTE. — Table 3 is published in its entirety in the electronic edition of the *Astrophysical Journal*. A portion is shown here for guidance regarding its form and content.